



Autophagy upregulation promotes macrophages to escape mesoporous silica nanoparticle (MSN)-induced NF-κB-dependent inflammation

Chen Xi¹ · Jie Zhou² · Shuzhang Du¹ · Shaojun Peng²

Received: 23 September 2015 / Revised: 19 January 2016 / Accepted: 21 January 2016 / Published online: 9 February 2016
© Springer International Publishing 2016

Abstract

Background Our previous studies (Int J Nanomed 10:22, 2015) have indicated that a single large dose of mesoporous silica nanoparticles (MSNs) can induce severe and selective nephrotoxicity, which is closely related to inflammation mediated by the NF-κB pathway. However, the effect of MSNs on other organs and the interactions of nanomaterials with biological systems remain rudimentary.

Objective This study aimed to clarify the biological behaviour and influence of MSNs on macrophages.

Methods The mice received a single intraperitoneal injection of a suspension of 150, 300 or 600 mg/kg MSNs, and RAW 264.7 cells were treated with MSNs at various

concentrations and times. Cell viability was determined by MTT assay and LDH release assay. The NF-κB pathway and the target proinflammatory cytokines IL-1 β and TNF- α were determined by western blotting or ELISA. Autophagy is considered as an emerging mechanism of nanomaterials. So the autophagic ultrastructural analysis, the determination of Beclin-1 and LC3 expression, and the calculation of LC3II dots were employed to verify autophagy activation. In addition, RNA interference, autophagy agonist and inhibitor were used to explore the role of autophagy in inflammation.

Results The results indicated that MSNs are internalized into macrophages and induce cytotoxicity in a dose- and time-dependent manner. The NF-κB pathway, IL-1 β and TNF- α were induced and released by MSNs. The levels of Beclin-1 and LC3II dots were obviously up-regulated by MSNs, which indicated that autophagy was induced in the MSN-treated cells. Moreover, the enhanced autophagy can attenuate the inflammation mediated by the NF-κB pathway, whereas the inhibition of autophagy can contribute to inflammation.

Conclusions In summary, our results suggest that autophagy may be a possible protective factor in inflammation induced by MSNs in macrophages.

Responsible Editor: John Di Battista.

C. Xi and J. Zhou contributed equally to this work.

Electronic supplementary material The online version of this article (doi:10.1007/s00011-016-0919-0) contains supplementary material, which is available to authorized users.

✉ Jie Zhou
zj9032@126.com

Shuzhang Du
du_shuzhang@126.com

Chen Xi
xichen00@126.com

Shaojun Peng
pengsj_yxy@126.com

¹ Pharmaceutical Department, The First Affiliated Hospital of Zhengzhou University, 450052 Zhengzhou, People's Republic of China

² School of Medicine, Yichun University, 576 XueFu Road, Yuanzhou District 336000 Yichun, People's Republic of China

Keywords Mesoporous silica nanoparticles (MSNs) · Inflammation · NF-κB · Autophagy · Macrophage

Abbreviations

3-MA	3-Methyladenine
BET	Brunauer–Emmett–Teller
BJH	Barrett–Joyner–Halenda
CTAB	Cetyltrimethyl ammonium bromide
DAPI	4,6-Diamidino-2-phenylindole dihydrochloride
DMEM	Dulbecco's modified Eagle medium
FBS	Fetal bovine serum

FITC	Fluorescein isothiocyanate
GFP	Green fluorescent protein
LDH	Lactate dehydrogenase
LPS	Lipopolysaccharide
MSNs	Mesoporous silica nanoparticles
mTOR	Mammalian target of rapamycin
MTT	3-(4,5)-Dimethylthiahiazo(-z-y1)-3,5-di-phenytetrazoliumromide
PBS	Phosphate-buffered saline
RAPA	Rapamycin
RES	Reticular endothelial system
SEM	Scanning electron microscopy
TEM	Transmission electron microscope
TEOS	Tetraethyl orthosilicate

Introduction

Mesoporous silica nanoparticles (MSNs) are emerging as a new and promising type of nanoparticle for drug delivery systems due to their special structures [1, 2]. However, the concerns associated with the biocompatibility caused by MSNs have also increased [3, 4], and standardized procedures for the evaluation of their toxicity have not been defined. It is well known that investigation of acute toxicity is the first step in the toxicological investigations of an unknown substance; thus, researchers should pay more attention to acute toxicity assessments. MSNs have been reported to cause injury in various organs, as observed in animal studies [5–7]. In our previous research, we found that MSNs intraperitoneally administered to mice have the potential to cause selective acute kidney toxicity at the early stage and result in the development of renal tubule interstitial fibrosis and that the acute nephrotoxicity observed was closely related to the NF-κB pathway [8].

Several studies on the potential toxicity of MSNs *in vivo* have focused on the biological behaviour of MSNs in reticular endothelial system (RES), which can non-selectively uptake and clear MSNs [9, 10]. It has been reported that liver lesions can be caused by a continuous intraperitoneal injection of MSNs into mice and that Kupffer cells play an important role in subacute liver injury [11]. Kupffer cells constitute the first macrophage population of the body to come in contact with bacteria, bacterial endotoxins and microbial debris derived from the gastrointestinal tract and transported to the liver via the portal vein. Kupffer cells are reported to be the major target cells of MSNs upon their entering the bloodstream [12]. Moreover, macrophages are more sensitive to MSNs than epithelial cells [13], and autophagy can be induced in macrophages by nanoparticles [14–16].

To date, nanoparticles have been considered a novel class of autophagy activators [17]. Autophagy, a highly regulated

cellular process for degrading proteins or organelles as well as the subsequent recycling of cellular products, plays an essential role in the maintenance of cellular homeostasis [18]. Autophagy can be induced by various stimuli, such as stress, cytokines, pathogens, aggregated proteins, and damaged or surplus organelles. Autophagy has been shown to have dual functions in the bio-effects of nanoparticles. Several recent studies have demonstrated that autophagy can enhance cellular function and survival by degrading damaged or unwanted proteins and organelles, by inhibiting apoptosis [14, 19, 20], and by inducing cell death [7, 21].

In our previous studies, we evaluated the acute toxicity of intraperitoneally administered MSNs *in vivo* and found that MSNs induced significant nephrotoxicity in mice. However, slight liver damage was observed during the total observation period because the liver has always been regarded as the major site for the removal of circulating macromolecules and microorganisms from the systemic circulation. There is consequently significant interest in how the liver escapes the damage induced by MSNs. This study is an extension of our previous study and aimed to tentatively understand the effects of autophagy on the biological behaviour of MSNs in the liver and the effects of autophagy on MSN-induced inflammation in macrophages. The present study can provide more persuasive evidence for the safety evaluation and risk management of nanomaterials.

Materials and methods

Materials

Cetyltrimethyl ammonium bromide (CTAB) and tetraethyl orthosilicate (TEOS) were purchased from Sigma-Aldrich (St. Louis, MO, US). Antibodies against the NF-κB pathway, Beclin-1 and LC3 were obtained from Cell Signaling Technology (Boston, MA, US). BAY 11-7082 (NF-κB inhibitor) was purchased from Beyotime Institute of Biotechnology (Haimeng, China). All other chemicals were of analytical grade and were purchased from commercial suppliers. The cell culture materials were purchased from NEST Biotech (Nest Biotechnology, Jiangsu, China).

Fabrication and characterization of MSNs

Mesoporous silica nanoparticles were synthesized in alkaline media according to a previous report with some modifications under our laboratory conditions [1]. TAB and TEOS were used as the template and silicon source, respectively. Briefly, in a three-necked flask, 1.0 g of CTAB and 0.28 g of sodium hydroxide were dissolved in 480 ml of water, and the resulting mixture was constantly stirred at 80 °C until all of the CTAB was dissolved and the

temperature became stable. Subsequently, 5 ml of TEOS was added dropwise to this solution, and the reaction solution was stirred for 2 h. The solid product was collected by centrifugation, washed with water until the filtrate was neutral, rinsed twice with alcohol, and being dried at 60 °C. The collected silica powder was then calcined at 550 °C for 8 h to completely eliminate the template. FITC-labelled MSNs were used in the cellular uptake experiment.

Adsorption–desorption of nitrogen

The pore characteristics of the MSNs were studied using a surface area and pore size analyser (ASAP 2020C, Micromeritics, US). Prior to characterization, the samples were degassed in vacuum at 300 °C for 12 h, whereas the drug-loaded samples were degassed at 40 °C for 12 h to avoid sublimation of carbamazepine. The specific surface area of the sample was calculated from the adsorption data obtained at the P/P_0 of nitrogen according to the multiple-point Brunauer–Emmett–Teller (BET) method. The pore volume was determined from the adsorption branch of the nitrogen adsorption–desorption isotherm curve at the $P/P_0 = 0.975$ signal point. The pore diameter was calculated from the adsorption branch of the isotherms using the Barrett–Joyner–Halenda (BJH) method.

Animals

Female BALB/C mice (6 weeks of age) were purchased from the Laboratory Animal Center in Sun Yat-sen University, Guangzhou, China. All of the mice were maintained in a specific pathogen-free animal room under controlled conditions at a temperature of 24 ± 2 °C and a humidity of 55 ± 15 % with a 12-h light/12-h dark cycle. Food and water were provided ad libitum. The animals were allowed to acclimatize to the environment for 4 days before the experiment. All of the animal experimental procedures in this study were performed in accordance with Sun Yat-Sen University Guidelines for the Welfare of Animals (Approval No: IACUC-2013-0904).

The mice were administered a single intraperitoneal injection of the MSN suspension in 5 % glucose at levels of 150, 300, and 600 mg/kg on day 1. Intraperitoneal injections of sterile 5 % glucose injection were also given to the mice as a control. The mortality and clinical manifestations were recorded. After 2 and 12 days, half of the animals in each group were sacrificed, and the organs were recovered.

Histopathological examinations

The liver was removed and immediately fixed in 4 % paraformaldehyde in PBS overnight. The tissues were embedded in paraffin blocks, sectioned into 3-μm sections and

mounted onto glass slides. After hematoxylin and eosin staining, the slides were observed, and photographs were taken using an optical microscope (Leica DM5000B, Germany).

TEM imaging of tissues

The liver tissues were dissected into 1-mm³ pieces and immersed in fresh 5 % glutaraldehyde in PBS overnight. The samples were treated at the Laboratory of Electron Microscopy of Sun Yat-Sen University. The TEM images were observed under a transmission electron microscope (Tecnai G² spirit Twin; FEI Ltd., Czech) operated at an accelerating voltage of 100 kV.

MTT and LDH leakage assay

RAW264.7 cells were obtained from the American Type Culture Collection (ATCC, US) and were seeded in a 96-well plate at a density of 4×10^3 cells/well. Twenty-four hours later, the cells were treated with the control (DMEM) or MSNs. The cell viability was determined using a 3-(4,5-dimethylthiazol-2-yl) -2,5-diphenyl tetrazolium bromide (MTT) assay, and the cell damage was assessed by determining the release of LDH from the cells using an LDH Detection Kit (Beyotime, Jiangsu, China) as previously reported [22].

Cellular uptake

The uptake of MSNs by RAW264.7 cells was visualized by confocal microscopy. The cells were grown on glass-bottomed dishes and incubated with FITC-labelled MSNs. The cell nuclei and cytoskeleton were stained with DAPI and Phalloidin-TRITC. Fluorescent images of the cells were obtained under a confocal microscope (CLSM; LSM710, Zeiss, Oberkochen, Germany).

Western blot

RAW264.7 cells were lysed on ice with Cell Protein Extraction Reagent (Pierce Chemical Co., Rockford, IL, US) to prepare the total protein fractions. The nuclear extracts were prepared using a Nuclear Extract kit (Active Motif, Carlsbad, CA, US) following the manufacturer's instructions. The lysate preparation and western blot analysis were performed as previously described [22].

Quantitative real-time PCR analysis (Q-PCR)

The total RNA was prepared using RNAiso Plus (TaKaRa, Japan), and cDNA was prepared from the total RNA using the PrimeScript RT Reagent Kit (TaKaRa, Japan) according to the manufacturer's instructions. The primers for real-time PCR analysis were obtained from Lee et al. [23]. The

subsequent PCR amplification was performed on a LightCycler 2.0 system (Roche Diagnostics, Basel, Switzerland).

Measurement of TNF- α and IL-1 β levels

RAW264.7 cells were seeded in 24-well black plates at a density of 4×10^4 cells/well and then exposed to MSNs, LPS, BAY11-7082, RAPA and 3-methyladenine (3-MA). Following treatment, 100 μ L of the supernatant was collected. The TNF- α and IL-1 β levels were detected using TNF- α and IL-1 β ELISA kits (Dakewe Biotech, Guangdong, China) according to the procedures provided by the manufacturers.

Transient transfection with plasmid and siRNA

The expression vectors for the GFP-LC3B vector and the empty vector (GFP) were kindly provided by Dr. Min Li (School of Pharmaceutical Science, Sun Yat-sen University). Negative control siRNA and Beclin-1 siRNA (F5'-G CUCCAUGCUUUGGCCAAUTT-3' and R5'-AUUGGCC AAAGCAUGGAGCTT-5') were obtained from Jima (Shanghai, China). The transient transfection and interference of cells were performed using Lipofectamine 2000 following the manufacturer's instructions.

Immunofluorescence staining

After treatment, RAW264.7 cells were fixed with 10 % paraformaldehyde in PBS, blocked with 10 % normal goat serum in PBS containing 0.3 % triton, and incubated with primary antibodies diluted in blocking buffer. After washing with PBS, the cells were incubated with Alexa Fluor 488-labeled goat anti-rabbit IgG. The coverslips were mounted in Prolong Gold anti-fade reagent with DAPI and inspected with a confocal microscope (Zeiss 710, Germany).

Statistical analysis

The SPSS v16.0 software (SPSS Inc., Chicago, IL, US) was used for the statistical analyses. The values are expressed as the mean \pm SD. The statistical comparisons were made using Student's *t* test and one-way analysis of variance (ANOVA) followed by Tukey's test. The level of significance was set to $p < 0.05$.

Results

Characterization of materials

The scanning electron microscopy (SEM; Fig. 1a) and transmission electron microscopy (TEM) images (Fig. 1b) showed that the MSNs were uniform, roughly spherical in

shape and ~ 150 nm in diameter. TEM was also employed to reveal the mesoporous structure in detail. The bright and dark areas indicated the pores and the silica walls, respectively, which could be clearly observed in the TEM images, confirming the hexagonal arrays of nanochannels.

To obtain more precise information on the structure of the MSNs, nitrogen adsorption–desorption measurements were performed, and these enabled the determination of the specific surface area, pore volume, and mesopore size distribution. As shown in Fig. 1c, the MSNs exhibited classical type-IV isotherms with H1-type hysteresis. According to the International Union of Pure and Applied Chemistry (IUPAC) classification [24], this suggests that the MSNs have uniform mesoporous channels and a relatively narrow pore size distribution in accordance with the TEM images. The corresponding pore size distribution (the insert of Fig. 1c) calculated from the adsorption branch of the isotherms showed a narrow pore size distribution. Moreover, the mean BET surface area, pore volume, and pore size of the MSNs were calculated to be $833.90\text{ m}^2/\text{g}$, $0.96\text{ cm}^3/\text{g}$, and 3.24 nm , respectively.

Effects of MSNs on the liver of Balb/c mice

The results shown in Fig. 2a indicate that the MSNs significantly increased the numbers and volume of Kupffer cells compared with the control. The effect of MSNs on Kupffer cells could be inferred from the images shown in Supplement 1. This assumption was also confirmed by TEM at the ultrastructural level (Fig. 2b–i). There was a large number of MSNs in Kupffer cells in the liver tissues of the middle-dose group both after 2 and 12 days, and the particle size of the trapped MSNs was virtually the same as that observed *in vitro* (Fig. 2e, i).

Cytotoxicity and cellular uptake of MSNs

The MSN-induced *in vitro* cytotoxicity was examined using RAW264.7 cells treated with various concentrations of MSNs for 3 and 24 h. The cell viability was measured using MTT assays. As shown in Fig. 3a, the MSNs reduced the viability of RAW264.7 cells in a time-dependent manner. After 24 h of exposure, the MSNs induced severe cytotoxicity in the RAW264.7 cells with an IC_{50} value of $214.12 \pm 31.35\text{ }\mu\text{g/mL}$. The cytotoxic effect of MSNs was evaluated through LDH leakage, which is a biomarker that indicates the integrity of the cell membrane. Twenty-four hours of incubation with various concentrations of MSNs (200–800 $\mu\text{g/mL}$) markedly induced the release of LDH (Fig. 3b). To observe the uptake of MSNs by RAW264.7 directly, we used confocal microscopy to visualize the distribution of MSNs at 15, 30, and 180 min. At 15 min, few green dots were observed inside the membrane, whereas at 30 min, a greater number of green dots had

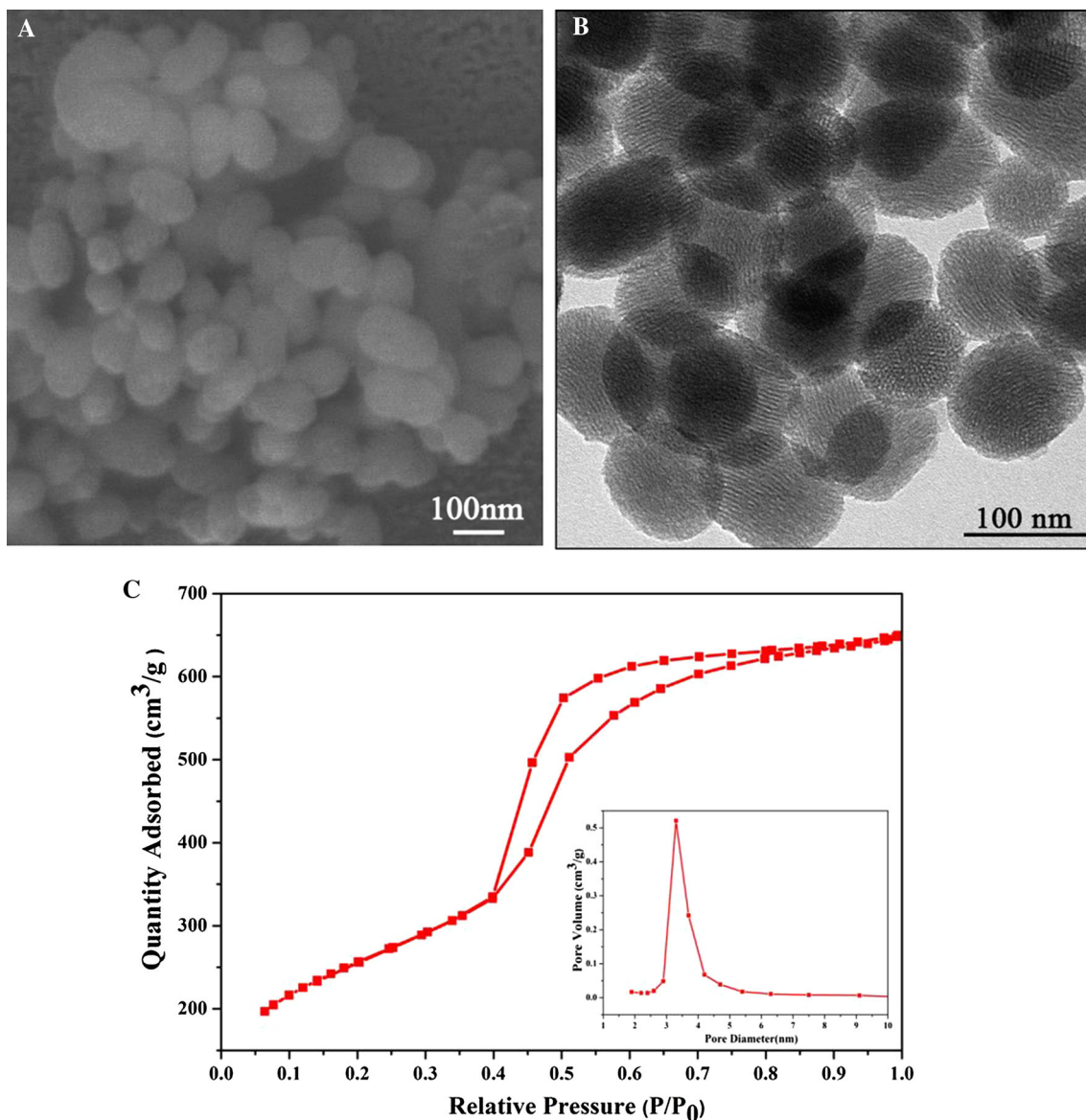


Fig. 1 Characterization of MSNs. Size distribution of MSNs following dispersion in PBS. Particle size distribution evaluated from the corresponding SEM (a) and TEM micrograph (b). Nitrogen

adsorption–desorption isotherms and pore size distribution (insert) of mesoporous silica nanoparticles. The average size of the MSNs was ~150 nm

moved from the membrane to the cytoplasm, and the cytoplasm was full of green dots at 180 min (Fig. 3c). This result indicated that the uptake of MSNs by RAW264.7 cells was time-dependent and showed saturation at ~180 min. These data demonstrate that the cytotoxicity induced by MSNs is associated with the internalization of MSNs, which is in agreement with previous reports [25].

Inflammation induced by MSNs via the NF-κB signalling pathway in RAW 264.7 cells

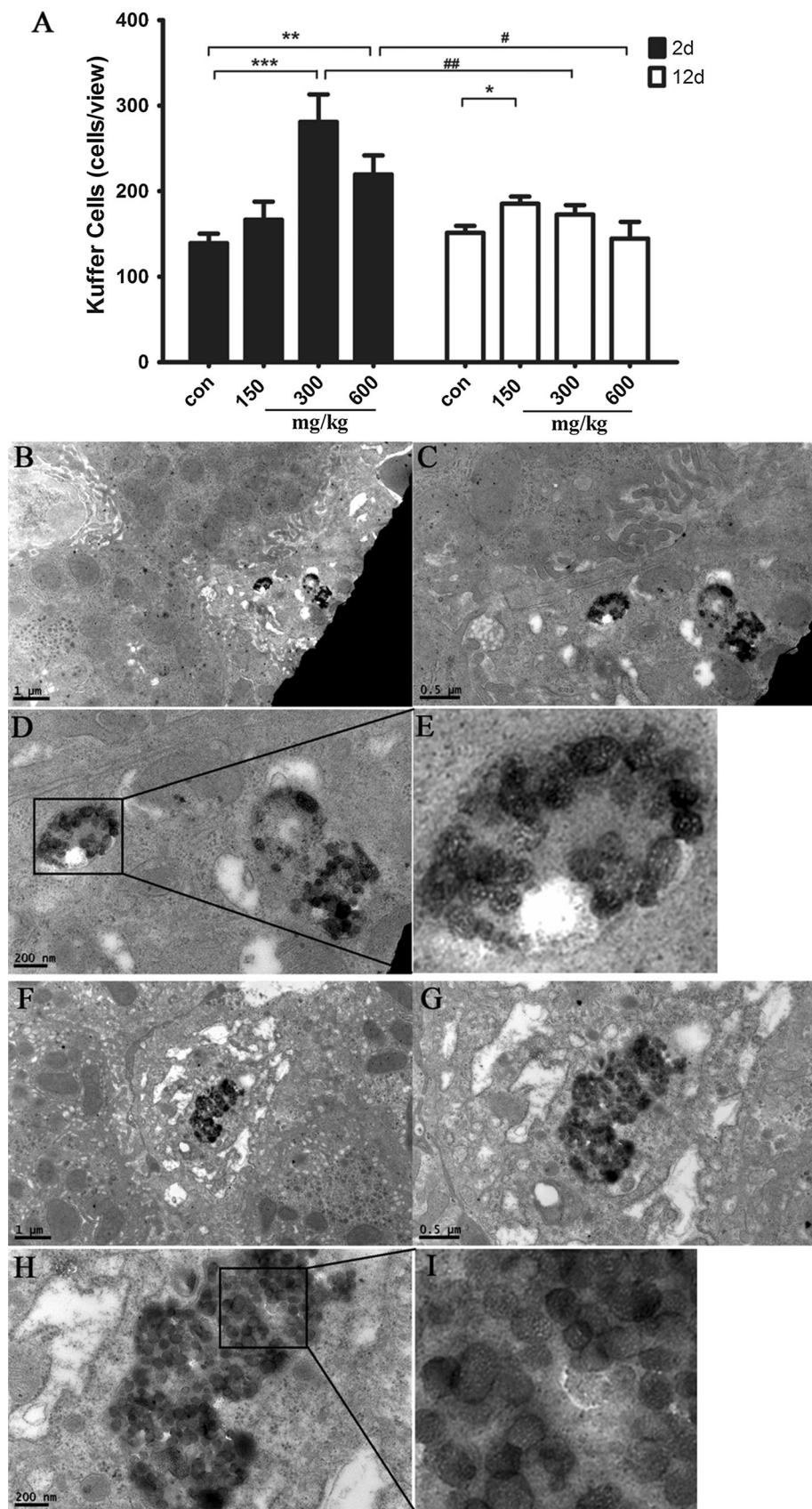
We previously showed the activation of the NF-κB inflammatory pathway in epithelial cells. Herein, to

investigate the inflammation induced by MSNs in RAW264.7 cells, we measured the activation of the NF-κB pathway.

Protein expression of the NF-κB pathway increased by MSNs

Because NF-κB activation is a rapid response, the protein levels were examined from 5 to 180 min. As shown in Fig. 4a, treatment with 400 μg/mL MSNs for 30 min can markedly increase the levels of phosphorylated IKKα/β, phosphorylated IκBα, and phosphorylated p65, but the total IKKα and p65 contents did not change throughout the

Fig. 2 Effect of MSNs on the liver of mice. The mice received a single intraperitoneal injection of a suspension of 150, 300 or 600 mg/kg MSNs in 5 % glucose on day 1. The control mice were administered intraperitoneal injections of sterile 5 % glucose. The mortality and clinical manifestations were recorded. After 2 and 12 days, half of each group was euthanized, and the serum and organs were recovered. The Kupffer cells from each group were quantitatively assessed by counting the number of cells in the H&E staining image, as shown by the arrows in Supplement 1, under 200 \times amplification. The data are expressed as the mean \pm SEM ($n = 3$, * $p < 0.05$, ** $p < 0.01$, and *** $p < 0.001$ intra-group, # $p < 0.05$, ## $p < 0.01$ among groups, ANOVA). Thin-section TEM images of the mouse liver 2 days (b–e) or 12 days (f–i) after the intraperitoneal injection of MSNs. KCs are normal in appearance after a single injection, 9700 \times (b, f); autophagosomes were formed in the KCs, 23,000 \times (c, g); MSNs were wrapped in autophagosomes, 46,000 \times (d, h); the structure of MSNs at scope magnifications (e, i). KC Kupffer cells. The scale bar is located in the lower left corner



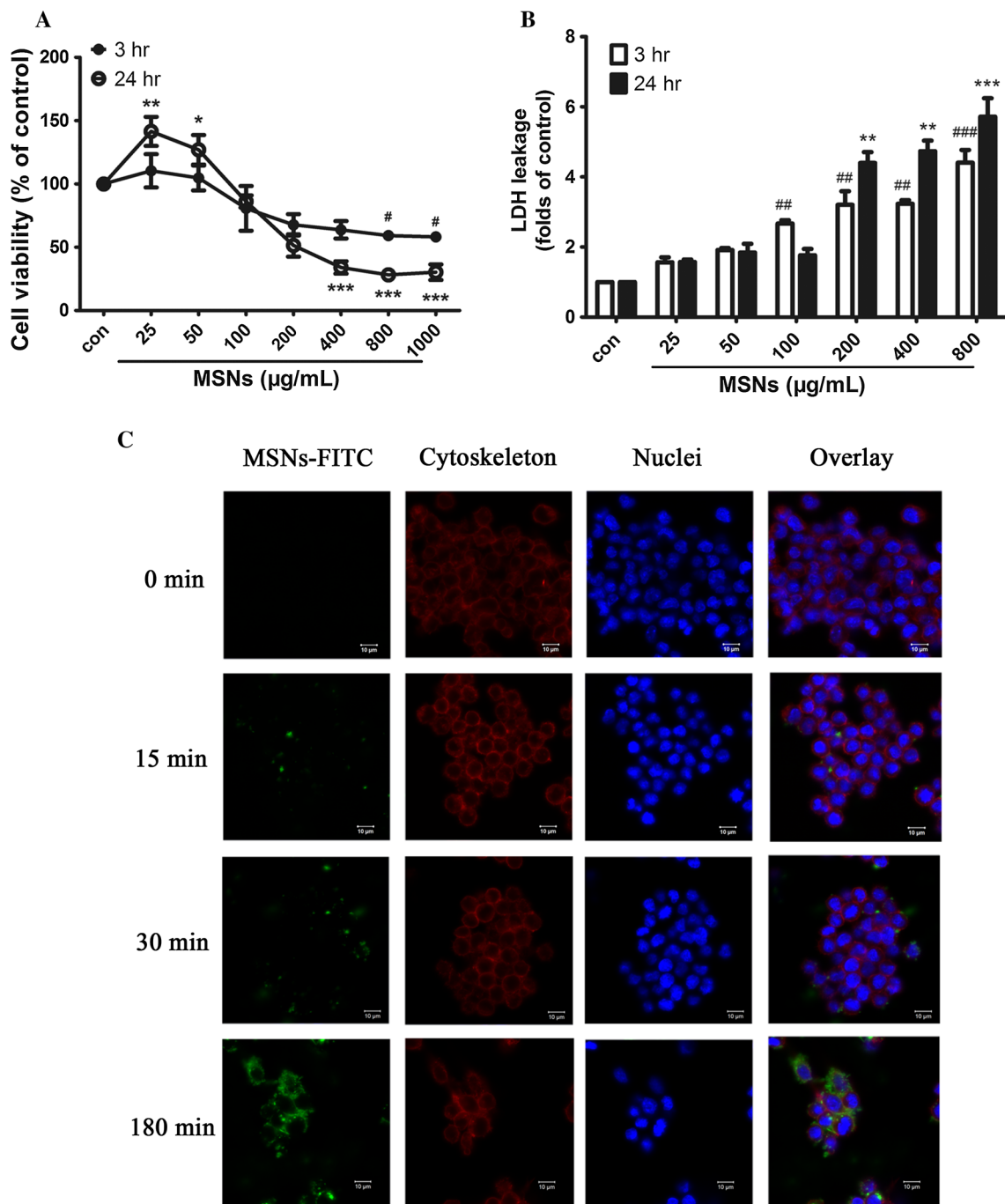


Fig. 3 Effects of MSNs on RAW 264.7 cells. RAW 264.7 cells were treated with MSNs at various concentrations for 3 and 24 h. Cell viability was determined by an MTT assay (a). The viability of the cells without MSNs treatment is defined as 100 %. For LDH release assay, RAW 264.7 was treated as mentioned for MTT assay, the conditional medium was harvested for LDH assay (b). The data are

expressed as the mean \pm SEM ($n = 3$, * $p < 0.05$, ** $p < 0.01$, and *** $p < 0.001$ vs. the control, ANOVA). Uptake of MSNs by RAW264.7 cells (c). MSNs are stained green (FITC staining), the cytoskeleton is stained red (Phalloidin-TRITC), and the nuclei are stained blue (DAPI)

treatment, whereas the total I κ B α content was significantly decreased after 1 h. Moreover, as shown in Fig. 4b, treatment with 50–400 $\mu\text{g/mL}$ MSNs for 30 min can increase the levels of phosphorylated IKK α/β , phosphorylated

I κ B α , and phosphorylated p65 in a dose-dependent manner, but incubation with 800 $\mu\text{g/mL}$ for the same time did not increase the levels of these proteins. None of the doses tested changed the total IKK α and p65 contents, whereas

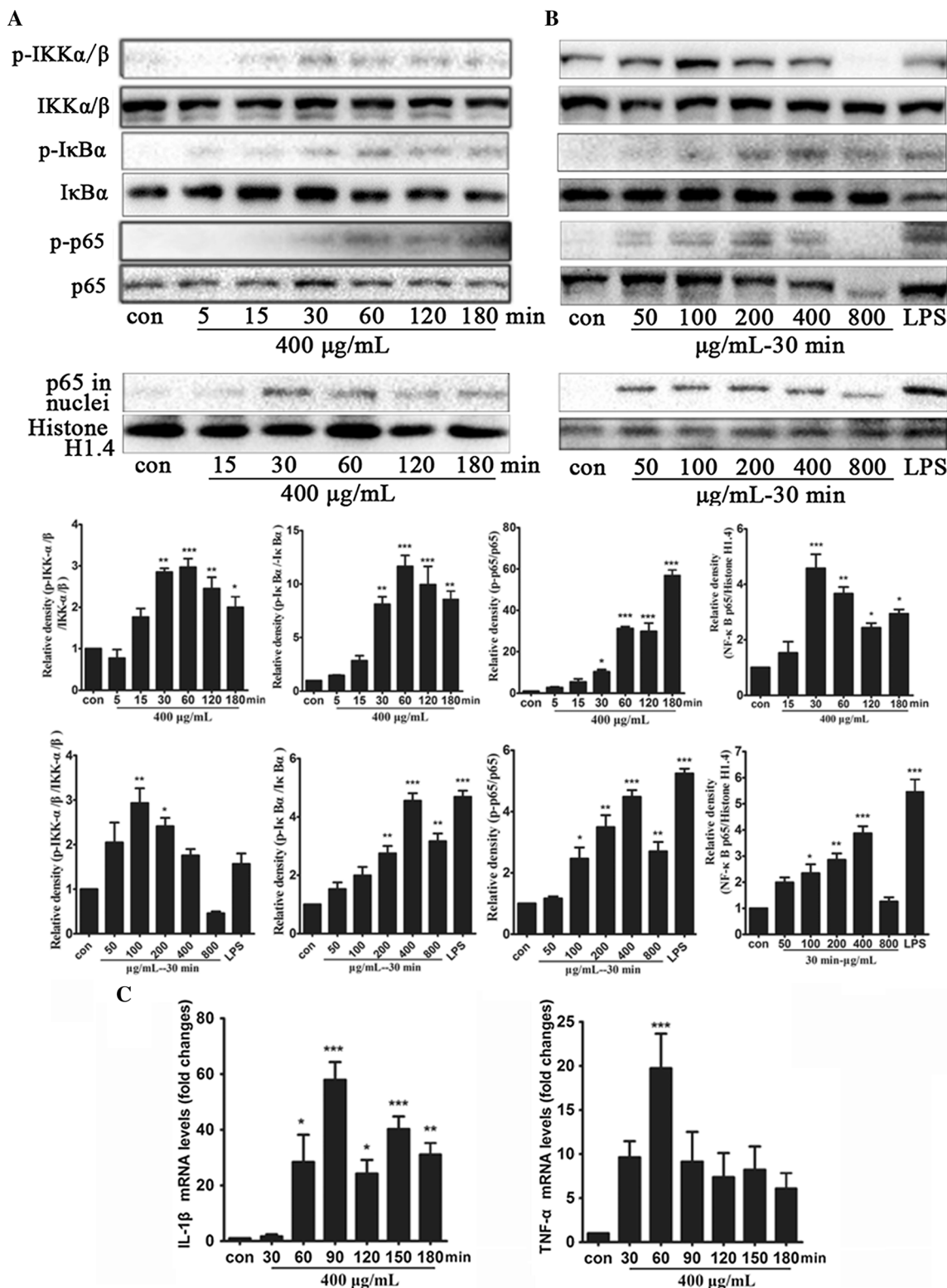


Fig. 4 Effects of MSNs on the activation of the NF- κ B signalling pathway. RAW 264.7 cells were treated with the indicated concentration of MSNs (50, 100, 200, 400, 800 μ g/mL) for 30 min or treated with 400 μ g/mL MSNs for the indicated time (5, 15, 30, 60, 120, 180 min). The proteins (p-IKK α/β , IKK α/β , p-I κ B α , I κ B α , p-p65, p65, Histone H1.4) were evaluated through western blotting. The cells were treated with 2 μ g/mL LPS as the positive control, and the blots were quantified by densitometry (**a**, **b**). Moreover, the cells were treated with 400 μ g/mL MSNs for the indicated time (5, 15, 30, 60, 120, 180 min). The mRNA expression levels of TNF- α and IL-1 β were analysed (**c**). The data are presented as the mean \pm SEM ($n = 3$, * $p < 0.05$, ** $p < 0.01$, and *** $p < 0.001$ vs. the control, ANOVA)

the total I κ B α level was decreased by treatment with 400 and 800 μ g/mL. Because NF- κ B p65 nuclear translocation is a key event in the activation of this pathway, we also examined NF- κ B p65 nuclear accumulation to investigate the effect of MSNs on NF- κ B activation. As shown in Fig. 4a, the NF- κ B p65 nuclear levels started to increase after 30 min, reached peak values after \sim 30–60 min of treatment, and then decreased. Moreover, treatment with various doses of MSNs for 30 min increased the nuclear levels of NF- κ B p65 in a dose-dependent manner, and peaks were reached at this time with the concentrations of 200–400 μ g/mL, as shown in Fig. 4b. LPS, which is a well-known NF- κ B activator, was utilized as a positive control.

Downstream proinflammatory cytokines of the NF- κ B pathway induced by MSNs

The activation of NF- κ B in response to MSNs was also evident by the induction of several NF- κ B target genes. As shown in Fig. 4c, the mRNA expression of TNF- α and IL-1 β was detected in the cells. During the time course, the expression of TNF- α started to increase at 30 min, peaked (20-fold induction) at 60 min, and then began to decrease, and this time course is similar to that obtained for NF- κ B nuclear accumulation. The levels of IL-1 β were markedly increased at 60 min, peaked (60-fold induction) at 90 min, decreased at 120 min, peaked again (45-fold induction) at 150 min, and then decreased again.

Alleviation of inflammation induced by MSNs through inhibition of the NF- κ B pathway in RAW 264.7 cells

To verify the NF- κ B activation induced by MSNs, we measured the NF- κ B nuclear accumulation induced by MSNs after treatment with the NF- κ B inhibitor BAY 11-7082, which is regarded as a common NF- κ B inhibitor, and found that it was downregulated in LPS-induced inflammation [26, 27]. As shown in Fig. 5a, pretreatment with BAY 11-7082 followed by co-incubation with MSNs

can reduce the nuclear translocation of NF- κ B p65 to the level observed in the control, and this effect significantly different from that observed in the MSN-treated group. As shown in Fig. 5b, the immunofluorescence staining results showed that the green staining of NF- κ B p65 was mainly gathered in the nuclei of the MSN- and LPS-treated groups, but dispersed in the cytoplasm of the control and NF- κ B-inhibited groups. In addition, BAY 11-7082 significantly downregulated the MSN-induced inflammatory factors, including the production and release of TNF- α and IL-1 β , as shown in Fig. 5c. In this study, LPS was utilized as a positive control.

Taken together, these results suggested that MSNs activates NF- κ B by triggering its nuclear translocation and protein accumulation in RAW264.7 cells, which leads to the transcriptional upregulation of NF- κ B-driven genes.

Activation of autophagy by MSNs

Expression of autophagy biomarkers increased by MSNs in RAW264.7 cells

It is known that nanoparticles are a new type of autophagy agonist due to their unique size. Several key molecules are involved in the autophagy process, and these include the processing of microtubule-associated protein 1-light chain 3-II (LC3-II), which is regarded as an autophagosome biomarker [28, 29]. Beclin-1 is a potential tumour suppressor gene that plays a positive role in the regulation of autophagy, because it can enhance the formation of autophagic vacuoles [30, 31]. Thus, we examined the Beclin-1 and LC3 accumulation after MSNs treatment to investigate the effect of MSNs on autophagy activation. The time courses of Beclin-1 and LC3 accumulation are shown in Fig. 6a. The western blot analysis shows that the expression of Beclin-1 and LC3 started to increase after 5 min, reached peak values 15–30 min after treatment with MSNs, and declined thereafter, and values similar to the basal levels were observed after 180 min of treatment. Moreover, treatment with 50–400 μ g/mL MSNs for 2 h increased Beclin-1 and LC3 expression in a dose-dependent manner, whereas treatment with 800 μ g/mL MSNs decreased Beclin-1 and LC3 expression, as shown in Fig. 6b.

GFP dots of LC3-II aggregation increased by MSNs in RAW 264.7 cells

LC3 is widely used as a hallmark of autophagy. LC3 (microtubule-associated protein 1 light chain 3), the mammalian homologue of the yeast ATG8 protein, is located in the autophagosome membrane [32]. Thus, to investigate the activation of autophagy, we measured the

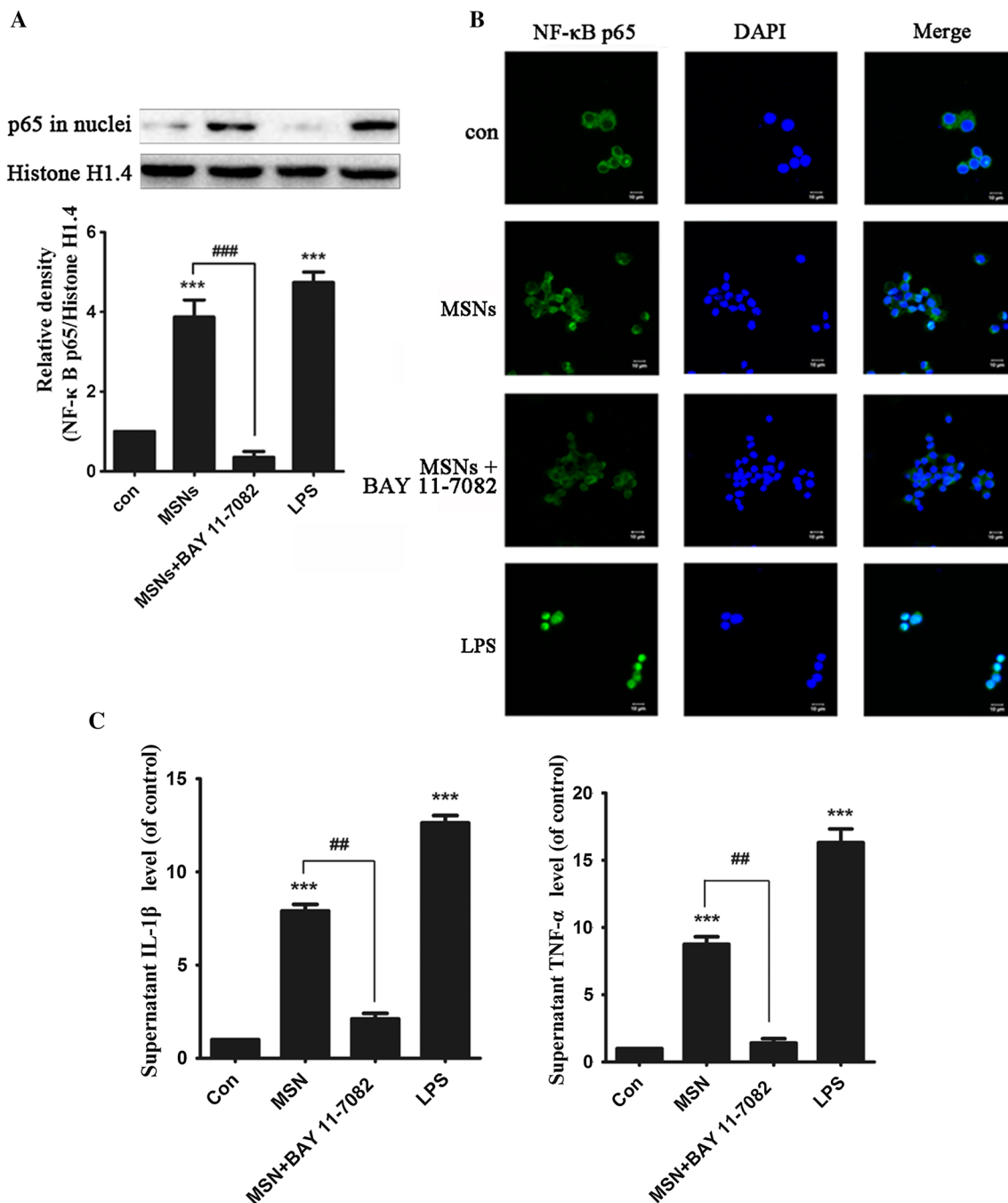


Fig. 5 Effect of BAY 11-7082 on NF- κ B activation induced by MSNs. The changes in the protein expression (**a**) and immunofluorescence staining (**b**) of NF- κ B p65 in the nuclei and cytoplasm were evaluated through western blotting and confocal microscopy. The production of TNF- α and IL-1 β was assessed by ELISA (**c**). MSNs: 400 μ g/mL MSNs for 2 h; LPS: 2 μ g/mL LPS for 30 min;

MSNs + BAY11-7082: pretreatment with 3 μ M BAY11-7082 for 1 h followed by treatment with MSNs for 2 h. BAY 11-7082, which is regarded as a common NF- κ B inhibitor. The data are presented as the mean \pm SEM ($n = 3$, *** $p < 0.001$ vs. the control, # $p < 0.01$, and # $#p < 0.001$ vs. MSNs, ANOVA)

punctate or vesicular spots (GFP-LC3 dots) under a fluorescence microscope after the GFP-LC3 plasmid was transfected into the cells [33]. As shown in Fig. 6c, RAW264.7 cells transfected with either GFP or GFP-LC3 and then treated with 100 μ g/mL MSNs-RITC for 2 h

exhibited GFP-LC3 dots in the cytoplasm that coincided with MSNs-RITC dots, but only diffuse fluorescence was observed in the control cells. This finding indicates that the MSNs and autophagosomes are co-localized in the cells; moreover, the results show that MSNs can induce LC3-II

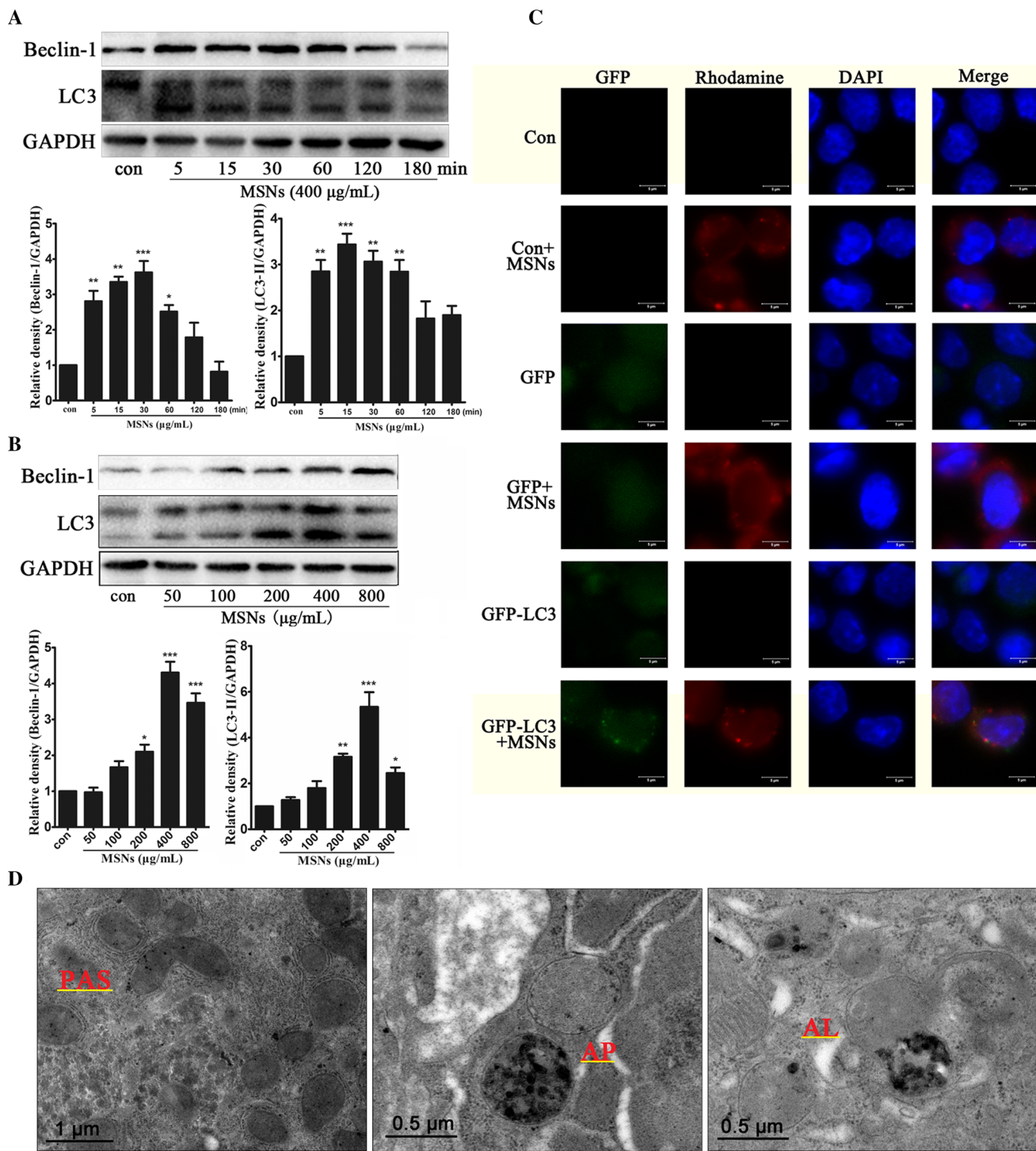


Fig. 6 Effects of MSNs on the activation of autophagy. RAW 264.7 cells were treated with the indicated concentration of MSNs (50, 100, 200, 400, 800 µg/mL) for 120 min or treated with 400 µg/mL MSNs for the indicated time (5, 15, 30, 60, 120, 180 min). The proteins (Beclin-1, LC3, GAPDH) were evaluated by western blotting (**a**, **b**). The cells were transfected with the GFP-LC3 plasmid. The immunofluorescence of LC3 dots and MSNs are shown through

confocal microscopy (**c**). Changes in autophagic structures (**d**) in liver tissues 2 days after an intraperitoneal injection of MSNs. *PAS* phagophore assembly site, *AP* autophagosome, *AL* autophagolysosome. The scale bar is located in the lower left corner. The data are presented as the mean ± SEM ($n = 3$, $*p < 0.05$, $**p < 0.01$, and $***p < 0.001$ vs. the control, ANOVA)

aggregation in RAW264.7 cells and can be wrapped into autophagosomes.

Autophagic structures induced by MSNs in the liver

The TEM examination (Fig. 6d) revealed the presence of a phagophore structure, a double-membrane autophagosome with engulfed damaged organelles and MSNs, and an autolysosome with a large vacuole containing a large amount of cellular debris and MSNs in Kupffer cells. The results demonstrated the induction of autophagic structures in the liver.

Alleviation of inflammation induced by MSNs in macrophages caused by autophagy

Effect of si-Beclin-1 transfection on inflammation induced by MSNs

To investigate the effect of autophagy knockdown in the inflammation induced by MSNs, we measured the changes in an autophagy biomarker and NF- κ B activation after si-Beclin-1 transfection. Beclin-1 is a homologous gene of the yeast autophagy genes Atg6/Vps30 that plays an important role in the development of autophagy [34] and regulates the formation and maturation of the autophagosome by mediating the location of some other autophagy proteins in the phagosomes [35]. Cells transfected with either si-con or si-Beclin-1 were treated with 400 μ g/mL MSNs for 2 h, as shown in Fig. 7a, and the knockdown of Beclin-1 significantly increased the degradation of I κ B α and the NF- κ B p65 nuclear accumulation caused by MSNs treatment compared with the control cells. This result suggests a protective role of autophagy against MSN-induced inflammation.

Effect of an autophagy agonist and an agonist blocker on inflammation induced by MSNs

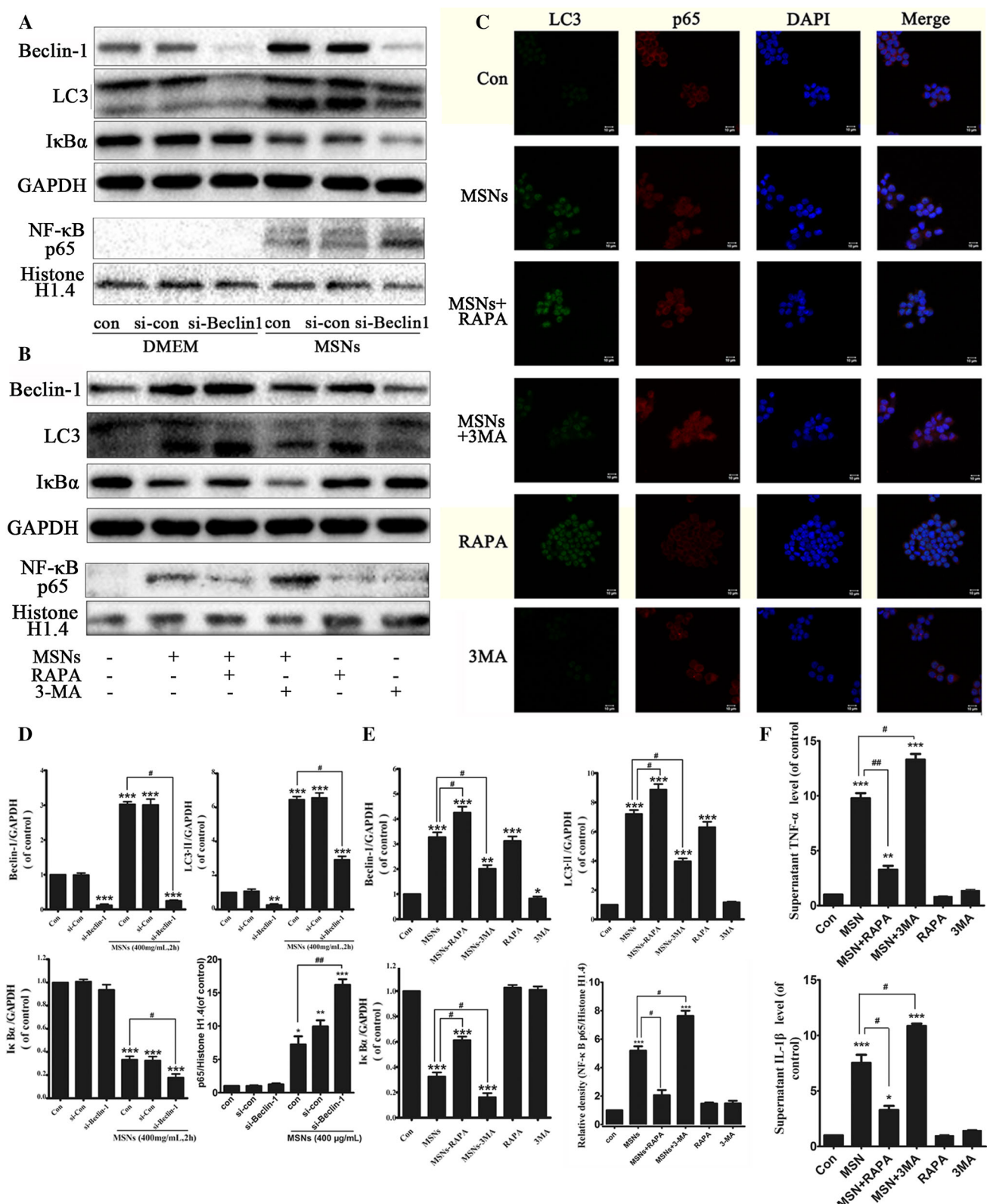
Rapamycin (RAPA) inhibits mTOR and thus enhances autophagy [36]. 3-MA inhibits autophagy by blocking autophagosome formation via the inhibition of type III phosphatidylinositol 3-kinases (PI-3Ks) [37]. To investigate the effect of autophagy activation or inhibition on the inflammation induced by MSNs, we measured the changes in an autophagy biomarker and NF- κ B activation after RAPA and 3-MA pretreatment. The cells were pretreated with either RAPA or 3-MA for 6 h and were then treated with 400 μ g/mL MSNs for 2 h, and the expression of Beclin-1, LC3, and I κ B α and the level of NF- κ B p65 nuclear accumulation were then determined. As shown in Fig. 7b, MSNs significantly increased the expression of Beclin-1 and LC3-II, the degradation of I κ B α and NF- κ B

Fig. 7 Intervention of autophagy on NF- κ B pathway activation induced by MSNs in RAW264.7 cells. RAW264.7 cells were pre-transfected with si-Beclin-1 for 48 h (a) or pretreated with RAPA and 3-MA for 6 h (b, c) and then treated with 400 μ g/mL MSNs for 2 h. The proteins were evaluated by western blotting. RAPA was used as an autophagy agonist, and 3-MA was used as an autophagy inhibitor. The protein expression (a, b, d, e) and immunofluorescence staining (c) of NF- κ B p65 and I κ B α are shown. The production of TNF- α and IL-1 β production (f) was assessed by ELISA. The data are presented as the mean \pm SEM ($n = 3$, * $p < 0.05$, ** $p < 0.01$, and *** $p < 0.001$ vs. the control, # $p < 0.05$, ## $p < 0.01$ vs. MSNs, ANOVA)

p65 nuclear translocation. The MSNs + RAPA group significantly increased the expression levels of Beclin-1 and LC3-II and decreased the degradation of I κ B α and NF- κ B p65 nuclear translocation induced by MSNs. The MSNs + 3-MA group increased the expression of Beclin-1 and LC3-II compared with control group, while the autophagy biomarkers were downregulated compared with MSNs group. Furthermore, pretreatment with 3-MA was found to promote the degradation of I κ B α and NF- κ B p65 nuclear translocation induced by MSNs. Treatment with only RAPA or 3-MA did not change the expression of I κ B α and the level of NF- κ B p65 nuclear translocation. A similar result was also observed through immunofluorescent staining, as shown in Fig. 7c. MSNs can induce LC3-II aggregation and NF- κ B p65 nuclear translocation and promote the development of inflammation. RAPA pretreatment attenuated the NF- κ B p65 nuclear translocation induced by MSNs, and 3-MA pretreatment enhanced the p65 nuclear translocation induced by MSNs. Treatment with only RAPA or 3-MA did not affect the NF- κ B p65 nuclear translocation in addition to the induction or inhibition of autophagy. In addition, the MSNs significantly increased the levels of inflammatory factors, including the production and release of TNF- α and IL-1 β . The pretreatment of cells with RAPA significantly increased the production and release of TNF- α and IL-1 β and decreased the release of TNF- α and IL-1 β induced by MSNs. Pretreatment with 3-MA increased the production and release of TNF- α and IL-1 β . These results indicate that enhanced autophagy may be an alternative for attenuating the inflammation induced by MSNs.

Discussion

MSNs are emerging as a new and promising type of nanoparticles for drug delivery systems due to their special structures [38–40]. Therefore, nanotoxicity research is gaining increasing attention. In our previous study [8], as part of a preclinical in vivo safety pharmacology evaluation, we reported the dose response, expanded the assessment of acute toxicology, and investigated the



nephrotoxicity mechanism of MSNs in mice. However, few liver pathologic changes were observed. In this study, we focused on the biological behaviour of MSNs in the liver and provide the first illustration of the influence of autophagy on MSN-induced macrophage inflammation in vitro. The results may provide a better understanding of the relationship between autophagy and inflammation induced by MSNs in mice.

To investigate the hypothesis, we first explored the bio-effect of MSNs. Compared with the control, the amount of Kupffer cells was significantly increased 2 days after treatment and was decreased after 12 days (Fig. 2a; Supplement 1). The pathological changes indicated that Kupffer cells are the target of MSNs in the liver and that MSNs can be excreted during 2 weeks [41, 42]. However, Kupffer cells were purified by attachment to a tissue culture plate, which is a sophisticated and time-consuming technique [43] and requires the killing of many animals. Due to animal ethics and convenience, we chose to use the murine monocyte-macrophage RAW264.7 cell line as a model to replace Kupffer cells. To provide closer insights into the MSN-induced biological effects on RAW264.7 cells, the cell viability and membrane integrity were measured as indicators of cytotoxicity. The data demonstrated that the MSN-induced cytotoxicity increased in a dose- and time-dependent manner (Fig. 3a, b). However, a small dose of MSNs appeared to increase the absorbance of MTT compared with the control, and this effect may be related to the MSN-induced enhancement of MTT formazan exocytosis [44]. Currently, the cellular uptake of nanoparticles is an important issue in designing suitable cell-tracking and drug-carrier nanomaterials systems [45] and may also be related to cytotoxicity [46]. Therefore, we examined the cellular uptake of silica nanoparticles. The TEM images showed the internalization and perinuclear localization of MSNs in the liver after 2 (Fig. 2b–e) and 12 days of exposure (Fig. 2f–i). In an in vitro study, we observed that the MSNs were not only absorbed by RAW264.7 cells in a time-dependent manner, but also distributed uniformly (Fig. 3c). These findings provide evidence to corroborate the hypothesis.

Some recent studies have shown that a severe inflammatory response induced by MSNs is a common initial step in their toxicity mechanism in vivo and in vitro [47]. Some studies have identified oxidative stress-related changes in gene expression and cell signalling pathways as the main traits of nanoparticle-induced cytotoxicity [48]. The NF-κB pathway plays an important role in both inflammatory and oxidative stress. Thus, to investigate whether the cytotoxicity induced by MSNs is associated with inflammation, we measured the activation of the NF-κB inflammatory pathway. The results showed that MSNs activate the NF-κB pathway from the top-down in RAW264.7 cells within a

short incubation time, induce the nuclear translocation of NF-κB p65 in both a dose-dependent (Fig. 5b) and time-dependent manner (Fig. 5a), and significantly increase the expression of NF-κB target genes, including TNF- α and IL-1 β (Fig. 5c). Because NF-κB pathway activation and the transcription of early target genes downstream of this pathway are important in the inflammatory process [49], the persistent activation of the NF-κB pathway is simply a necessary condition to tissue injury [50]. To investigate the role of the NF-κB pathway in the inflammation caused by MSNs, we used BAY 11-7082, an inhibitor of the NF-κB pathway. This inhibitor can effectively prevent the phosphorylation of IκB α by cytokines and thereby decreases the nuclear translocation of NF-κB p65. Herein, BAY 11-7082 decreased the nuclear translocation of p65 (Fig. 5a, b) as well as the expression of the NF-κB target genes IL-1 β and TNF- α (Fig. 5c). These results raise the possibility that MSNs can activate the NF-κB pathway and that this effect is closely related to cytotoxicity in RAW264.7 cells.

To date, autophagy is considered one of the emerging mechanisms induced by nanomaterials. However, the detailed mechanisms of nanomaterial-induced autophagy have not been fully investigated [7]. Ultrastructural analysis has been recommended as the golden standard for autophagy diagnosis [51], and the TEM observations showed the existence of a phagophore, autophagosome and autolysosome structure, which indicates that autophagy was activated by MSNs in Kupffer cells (Fig. 6d). As is well known, Beclin-1 and LC3 proteins are required for autophagy. Beclin-1 is an autophagy-related gene (Atg6) that can initiate autophagosome formation during autophagy when upregulated in mammalian cells [35]. LC3, a full-length cytosolic protein expressed in most cell types, is present in the LC3I form under normal conditions. Upon the induction of autophagy, LC3 is proteolytically cleaved to generate LC3II on autophagosomal membranes. Both Beclin-1 and LC-3 were increased in a dose- and time-dependent manner after treatment with MSNs (Fig. 6a, b). Thus, in cells transfected with the GFP-LC3 plasmid, the induction of autophagy results in GFP-LC3 dot fluorescence [52], and several GFP-LC3 dots that appeared in the RAW264.7 cytoplasm coincided with MSNs-RITC dots (Fig. 6c). All of these results indicate that MSNs can induce autophagy in macrophages both in vivo and in vitro.

In consideration of the controversial role of autophagy, which can be maladaptive in some contexts and beneficial in others, we investigated the relationship between autophagy and inflammation in MSN-treated RAW264.7 cells. To further explore the role of autophagy in MSN-induced inflammation, autophagy was first manipulated using a genetic approach. We knocked down Beclin-1 in RAW264.7 cells by RNA interference to block autophagy [53]. Compared with the time course in which the LC3II

and Beclin-1 protein levels decrease, the suppression of autophagy by the knockdown of Beclin-1 markedly enhanced the degradation of I κ B α and the nuclear translocation of NF- κ B p65 (Fig. 7a, d). RAPA is a well-known specific negative regulator of the mTOR signalling pathway [54], which plays a key role in the process of autophagy [55]. In contrast, 3-MA is a common inhibitor of autophagy. In this study, we pretreated cells with RAPA to induce autophagy and with 3-MA to downregulate autophagy prior to treatment with MSNs. The results showed that, in addition to upregulating the expression of LC-3 and Beclin-1, pretreatment with RAPA can attenuate the degradation of I κ B α and the nuclear translocation of NF- κ B p65 (Fig. 7b, c, e) and decrease the production and release of the proinflammatory cytokines IL-1 β and TNF- α (Fig. 7f). In contrast, pretreatment with 3-MA can aggravate the above-described process. These findings indicate that autophagy activation can attenuate the inflammation induced by MSNs in macrophages. As a type of exogenous compound, MSNs can promote Kupffer cell transformation and proliferation (Fig. 2a) and release various molecules, including TNF- α and IL-1 β , which play important roles in liver injury and hepatocellular necrosis [56, 57]. As the major tissue macrophages localized within the liver [58], Kupffer cells are sensitive to MSNs and critical for the endocytosis, retention and removal of nanoparticles in the liver [59, 60]. In the present study, autophagy activation was found to significantly downregulate the inflammation induced by MSNs in macrophages (Fig. 7). Thus, we conclude that enhanced autophagy can protect against the inflammation induced by MSNs in Kupffer cells. In addition, autophagy and potentially lysosomal recycling contribute to the phagocytosis and internalization of MSNs into macrophages [13]. Some recent studies have shown that a variety of nanoparticles can induce autophagy preceding or accompanied by apoptosis or inflammatory responses [61, 62], but few of these illuminate the relationship between autophagy and inflammation or apoptosis. Lin and coworkers found that autophagy induced by nanoparticles is cytoprotective in cancer cells [63], which is in accordance with our results. Consistent with previous studies, our data confirm that MSN-induced inflammation can be modified by autophagy, and a tentative inference from this work is that MSN-induced autophagy may be the mechanism underlying the escape of the liver from the inflammatory toxicity induced by MSNs.

Conclusions

Overall, both in vitro and in vivo studies indicated that inflammation mediated by the NF- κ B pathway, as well as autophagy, can be induced by MSNs in macrophages.

Moreover, several lines of evidence obtained in this study indicate that cytoprotective autophagy may play a positive role in attenuating the inflammation induced by MSNs and may be the mechanism underlying the escape of the liver from the damage induced by MSNs. In addition, the upregulation of autophagy may be a useful strategy for decreasing the toxicity of MSNs in biological applications, and the mechanism underlying the regulatory role of autophagy in MSN-induced inflammation in animal models will be investigated in our future research. In summary, the findings presented in this report are particularly significant because they indicate a potential protective role for autophagy against the inflammation induced by a large dose of MSNs. Thus, we hypothesize that a better understanding of the implication and biological significance of MSN-induced autophagy and inflammation will help us understand the risks associated with its applications and allow the development of safer nanoparticles.

Compliance with ethical standards

Conflict of interest None.

References

1. Liu H, et al. Multifunctional gold nanoshells on silica nanorattles: a platform for the combination of photothermal therapy and chemotherapy with low systemic toxicity. *Angew Chem Int Ed Engl.* 2011;50(4):891–5.
2. Slowing II, et al. Mesoporous silica nanoparticles as controlled release drug delivery and gene transfection carriers. *Adv Drug Deliv Rev.* 2008;60(11):1278–88.
3. Slowing II, et al. Mesoporous silica nanoparticles for reducing hemolytic activity towards mammalian red blood cells. *Small.* 2009;5(1):57–62.
4. Tao Z, et al. Mesoporous silica nanoparticles inhibit cellular respiration. *Nano Lett.* 2008;8(5):1517–26.
5. Fu C, et al. The absorption, distribution, excretion and toxicity of mesoporous silica nanoparticles in mice following different exposure routes. *Biomaterials.* 2013;34(10):2565–75.
6. Hassankhani R, et al. In vivo toxicity of orally administrated silicon dioxide nanoparticles in healthy adult mice. *Environ Sci Pollut Res Int.* 2015;22(2):1127–32.
7. Duan J, et al. Silica nanoparticles enhance autophagic activity, disturb endothelial cell homeostasis and impair angiogenesis. Part Fibre Toxicol. 2014;11:50.
8. Xi C, et al. Renal interstitial fibrosis induced by high-dose mesoporous silica nanoparticles via the NF- κ B signaling pathway. *Int J Nanomed.* 2015;10:22.
9. Fischer HC, Chan WC. Nanotoxicity: the growing need for in vivo study. *Curr Opin Biotechnol.* 2007;18(6):565–71.
10. Soo-Jin C, Jae-Min O, Jin-Ho C. Human-related application and nanotoxicology of inorganic particles: complementary aspects. *J Mater Chem.* 2008;18(0959–9428):6.
11. Liu T, et al. Pathological mechanisms of liver injury caused by continuous intraperitoneal injection of silica nanoparticles. *Biomaterials.* 2012;33(7):2399–407.
12. Liu T, et al. Single and repeated dose toxicity of mesoporous hollow silica nanoparticles in intravenously exposed mice. *Biomaterials.* 2011;32(6):1657–68.

13. Herd HL, Malugin A, Ghandehari H. Silica nanoconstruct cellular toleration threshold in vitro. *J Control Release*. 2011;153(1):40–8.
14. Park EJ, et al. Magnetic iron oxide nanoparticles induce autophagy preceding apoptosis through mitochondrial damage and ER stress in RAW264.7 cells. *Toxicol In Vitro*. 2014;28(8):1402–12.
15. Roy R, et al. Zinc oxide nanoparticles induce apoptosis by enhancement of autophagy via PI3 K/Akt/mTOR inhibition. *Toxicol Lett*. 2014;227(1):29–40.
16. Li R, et al. Interference in autophagosome fusion by rare earth nanoparticles disrupts autophagic flux and regulation of an interleukin-1 β producing Inflammasome. *ACS Nano*. 2014;8(10):10280–92.
17. Zabirnyk O, Yezhelyev M, Seleverstov O. Nanoparticles as a novel class of autophagy activators. *Autophagy*. 2007;3(3):278–81.
18. Teng RJ, et al. Cross talk between NADPH oxidase and autophagy in pulmonary artery endothelial cells with intrauterine persistent pulmonary hypertension. *Am J Physiol Lung Cell Mol Physiol*. 2012;302(7):L651–63.
19. Nowak JS, et al. Silica nanoparticle uptake induces survival mechanism in A549 cells by the activation of autophagy but not apoptosis. *Toxicol Lett*. 2014;224(1):84–92.
20. Hussain S, Garantziotis S. Interplay between apoptotic and autophagy pathways after exposure to cerium dioxide nanoparticles in human monocytes. *Autophagy*. 2013;9(1):101–3.
21. Stern ST, Adiseshaiah PP, Crist RM. Autophagy and lysosomal dysfunction as emerging mechanisms of nanomaterial toxicity. *Part Fibre Toxicol*. 2012;9:20.
22. Zhou J, et al. Triptolide-induced oxidative stress involved with Nrf2 contribute to cardiomyocyte apoptosis through mitochondrial dependent pathways. *Toxicol Lett*. 2014;230(3):454–66.
23. Lee S, Yun HS, Kim SH. The comparative effects of mesoporous silica nanoparticles and colloidal silica on inflammation and apoptosis. *Biomaterials*. 2011;32(35):9434–43.
24. Everett DH. IUPAC manual of symbols and terminology. *Pure Appl Chem*. 1972;31:61.
25. Sun W, et al. Endocytosis of a single mesoporous silica nanoparticle into a human lung cancer cell observed by differential interference contrast microscopy. *Anal Bioanal Chem*. 2008;391(6):2119–25.
26. Zhang JY, et al. Methyl-1-hydroxy-2-naphthoate, a novel naphthol derivative, inhibits lipopolysaccharide-induced inflammatory response in macrophages via suppression of NF- κ B, JNK and p38 MAPK pathways. *Inflamm Res*. 2011;60(9):851–9.
27. Wang QS, et al. Dietary blue pigments derived from genipin, attenuate inflammation by inhibiting LPS-induced iNOS and COX-2 expression via the NF- κ B inactivation. *PLoS ONE*. 2012;7(3):e34122.
28. Tanida I. Autophagosome formation and molecular mechanism of autophagy. *Antioxid Redox Signal*. 2011;14(11):2201–14.
29. Yoshioka A, et al. LC3, an autophagosome marker, is highly expressed in gastrointestinal cancers. *Int J Oncol*. 2008;33(3):461–8.
30. Guo GF, et al. Autophagy-related proteins Beclin-1 and LC3 predict cetuximab efficacy in advanced colorectal cancer. *World J Gastroenterol*. 2011;17(43):4779–86.
31. Wei Y, et al. EGFR-mediated Beclin 1 phosphorylation in autophagy suppression, tumor progression, and tumor chemoresistance. *Cell*. 2013;154(6):1269–84.
32. Kabeya Y, et al. LC3, a mammalian homologue of yeast Apg8p, is localized in autophagosome membranes after processing. *EMBO J*. 2000;19(21):5720–8.
33. Kimura S, et al. Monitoring autophagy in mammalian cultured cells through the dynamics of LC3. *Methods Enzymol*. 2009;452:1–12.
34. Hönscheid P, Datta K, Muders MH. Autophagy: detection, regulation and its role in cancer and therapy response. *Int J Radiat Biol*. 2014;90(8):628–35.
35. Ryter SW, Cloonan SM, Choi AM. Autophagy: a critical regulator of cellular metabolism and homeostasis. *Mol Cells*. 2013;36(1):7–16.
36. Pan T, et al. Rapamycin protects against rotenone-induced apoptosis through autophagy induction. *Neuroscience*. 2009;164(2):541–51.
37. Wu YT, et al. Dual role of 3-methyladenine in modulation of autophagy via different temporal patterns of inhibition on class I and III phosphoinositide 3-kinase. *J Biol Chem*. 2010;285(14):10850–61.
38. Hwang AA, et al. Functional nanovalves on protein-coated nanoparticles for in vitro and in vivo controlled drug delivery. *Small*. 2015;11(3):319–28.
39. Rogers R, et al. The practicality of mesoporous silica nanoparticles as drug delivery devices and progress toward this goal. *AAPS PharmSciTech*. 2014;15:1–9.
40. Pan L, et al. MSN-mediated sequential vascular-to-cell nuclear-targeted drug delivery for efficient tumor regression. *Adv Mater*. 2014;26(39):6742–8.
41. Nabeshi H, et al. Systemic distribution, nuclear entry and cytotoxicity of amorphous nanosilica following topical application. *Biomaterials*. 2011;32(11):2713–24.
42. Nabeshi H, et al. Amorphous nanosilicas induce consumptive coagulopathy after systemic exposure. *Nanotechnology*. 2012;23(4):045101.
43. Li PZ, et al. An efficient method to isolate and culture mouse Kupffer cells. *Immunol Lett*. 2014;158(1–2):52–6.
44. Fisichella M, et al. Mesoporous silica nanoparticles enhance MTT formazan exocytosis in HeLa cells and astrocytes. *Toxicol In Vitro*. 2009;23(4):697–703.
45. Smith AM, et al. Bioconjugated quantum dots for in vivo molecular and cellular imaging. *Adv Drug Deliv Rev*. 2008;60(11):1226–40.
46. Tao Z, et al. Mesoporosity and functional group dependent endocytosis and cytotoxicity of silica nanomaterials. *Chem Res Toxicol*. 2009;22(11):1869–80.
47. Mühlfeld C, Gehr P, Rothen-Rutishauser B. Translocation and cellular entering mechanisms of nanoparticles in the respiratory tract. *Swiss Med Wkly*. 2008;138(27–28):387–91.
48. Oberdörster G, Oberdörster E, Oberdörster J. Nanotoxicology: an emerging discipline evolving from studies of ultrafine particles. *Environ Health Perspect*. 2005;113(7):823–39.
49. Kang JL, et al. Src tyrosine kinases mediate crystalline silica-induced NF- κ B activation through tyrosine phosphorylation of IkappaB-alpha and p65 NF- κ B in RAW 264.7 macrophages. *Toxicol Sci*. 2006;90(2):470–7.
50. Mirza A, et al. A role for tissue transglutaminase in hepatic injury and fibrogenesis, and its regulation by NF- κ B. *Am J Physiol*. 1997;272(2 Pt 1):G281–8.
51. Di Gioacchino M, et al. Autophagy as an ultrastructural marker of heavy metal toxicity in human cord blood hematopoietic stem cells. *Sci Total Environ*. 2008;392(1):50–8.
52. Mizushima N, Yoshimori T, Levine B. Methods in mammalian autophagy research. *Cell*. 2010;140(3):313–26.
53. Yang M, et al. Chloroquine inhibits HMGB1 inflammatory signaling and protects mice from lethal sepsis. *Biochem Pharmacol*. 2013;86(3):410–8.
54. Hartford CM, Ratain MJ. Rapamycin: something old, something new, sometimes borrowed and now renewed. *Clin Pharmacol Ther*. 2007;82(4):381–8.
55. Zoncu R, Efeyan A, Sabatini DM. mTOR: from growth signal integration to cancer, diabetes and ageing. *Nat Rev Mol Cell Biol*. 2011;12(1):21–35.

56. Kmiec Z, et al. Cooperation of liver cells in health and disease. *Adv Anat Embryol Cell Biol.* 2001;161:1–151 (**III–XIII**).
57. Hoek JB, Pastorino JG. Ethanol, oxidative stress, and cytokine-induced liver cell injury. *Alcohol.* 2002;27(1):63–8.
58. Tsutsui H, Nishiguchi S. Importance of Kupffer cells in the development of acute liver injuries in mice. *Int J Mol Sci.* 2014;15(5):7711–30.
59. Nishimori H, et al. Histological analysis of 70-nm silica particles-induced chronic toxicity in mice. *Eur J Pharm Biopharm.* 2009;72(3):626–9.
60. Xue Y, et al. SiO₂ nanoparticle-induced impairment of mitochondrial energy metabolism in hepatocytes directly and through a Kupffer cell-mediated pathway in vitro. *Int J Nanomedicine.* 2014;9:2891–903.
61. Duan J, et al. Silica nanoparticles induce autophagy and endothelial dysfunction via the PI3 K/Akt/mTOR signaling pathway. *Int J Nanomedicine.* 2014;9:5131–41.
62. Qin Y, et al. Graphene quantum dots induce apoptosis, autophagy, and inflammatory response via p38 mitogen-activated protein kinase and nuclear factor- κ B mediated signaling pathways in activated THP-1 macrophages. *Toxicology.* 2015;327: 62–76. doi:[10.1016/j.tox.2014.10.011](https://doi.org/10.1016/j.tox.2014.10.011).
63. Lin J, et al. Inhibition of autophagy enhances the anticancer activity of silver nanoparticles. *Autophagy.* 2014;10(11):2006–20.